





# Cooperative Gelation of Syndiotactic Polystyrene and Low Molecular Weight PEGDME

<sup>1</sup>Jülich Centre for Neutron Science (JCNS) at Heinz Maier-Leibnitz Zentrum (MLZ), Forschungszentrum Jülich GmbH, Garching, Germany | <sup>2</sup>Centre for Nanoscience and Nanotechnology, Sathyabama Institute of Science and Technology, Chennai, Tamil Nadu, India | <sup>3</sup>Institute of High Energy Physics (IHEP), Chinese Academy of Sciences (CAS), Beijing, China | <sup>4</sup>Spallation Neutron Source Science Center, Dongguan, China | <sup>5</sup>German Engineering Materials Science Centre (GEMS) at Heinz Maier-Leibnitz Zentrum (MLZ), Helmholtz-Zentrum Hereon, Garching, Germany | <sup>6</sup>Dipartimento di Chimica e Biologia "Adolfo Zambelli", Università di Salerno, Fisciano, Italy | <sup>7</sup>Jülich Centre for Neutron Science (JCNS), Forschungszentrum Jülich GmbH, Jülich, Germany

Correspondence: Aurel Radulescu (a.radulescu@fz-juelich.de)

Received: 19 March 2025 | Revised: 5 June 2025 | Accepted: 16 June 2025

Keywords: contrast matching SANS | FTIR | semi-crystalline polymers | thermo-reversible gels

#### **ABSTRACT**

The cooperative gelation of sPS with the short PEGDME molecules (molecular weight  $M_{\rm W}=1.5~{\rm kg~mol^{-1}}$ ) from a common THF solution is driven by the gelation tendency of sPS at a temperature around 40°C. The crystalline junctions in the wet gel are fibrillar morphologies, which are typically composed of sPS and PEG molecules, as shown by contrast variation SANS, and consist of sPS, which co-crystallizes in d-form with the solvent molecules, and to a certain extent with PEGDME molecules, as demonstrated by the conformational change of both polymer types from an amorphous to a helical form when the gelation temperature is exceeded, which was observed by in situ FTIR. XRD and SEM on drying gels have shown that the large-scale morphology of dry gels, when the polymer strands collapse and crystalline polymer strands are formed, is determined by the presence and length of the PEGDME molecules. While the sPS dry gel exhibits a more homogeneous distribution of polymer strands and well-defined pores, the polymer strands of the gel with short PEGDME connect at one end to form "tufted" macroassemblies, which, due to the additional co-crystallization of PEGDME with sPS, leads to very large pores and voids.

# 1 | Introduction

Syndiotactic polystyrene (sPS) is a relatively new material [1] that exhibits some very interesting properties: i) a complex polymorphic behavior, including five different crystalline forms in which the chains either adopt a planar zigzag ( $\alpha$ - and  $\beta$ -forms) or a TTGG helix ( $\gamma$ -,  $\delta$ -, and  $\varepsilon$ -forms) conformation [2–5] and ii) the ability to form various types of co-crystalline (clathrate) phases with a large number of small organic molecules that can be incorporated as guests into the cage- or channel-like cavities between the polymer helices of the  $\delta$ - or  $\varepsilon$ -forms [6–10]. Depending on the type of solvent, helical co-crystalline  $\delta$ -

and  $\varepsilon$ -forms can be produced by solvent-induced crystallization in cast films or by exposing amorphous films to solvents in vapor or liquid state. Furthermore, the initial guest molecules in sPS co-crystals can be smoothly replaced by other molecules by exposing them to vapors or liquid of the new solvent [10–16]. The clathrate forms are interesting for applications in which active guests can be incorporated into the sPS films, resulting in advanced materials for optical and magnetic applications [17–20], while the emptied clathrates, which can be produced with suitable methods for guest extraction [10, 11], can be used as molecular sieves [21] for water purification of chlorinated hydrocarbons.

This is an open access article under the terms of the Creative Commons Attribution License, which permits use, distribution and reproduction in any medium, provided the original work is properly cited.

© 2025 The Author(s). Macromolecular Materials and Engineering published by Wiley-VCH GmbH

Linear polyethylene glycols (PEG) with molecular weight  $(M_W)$  up to 1000 g mol $^{-1}$  could also be loaded as guests in sPS  $\delta$  cocrystals following the guest-exchange mechanism [22], as also confirmed by simultaneous FTIR and SANS characterization [23, 24]. The incorporation of PEG into sPS gels and films can lead to polymer nanocomposites that can make the sPS hydrophilic [25], which would increase and diversify the application potential of the otherwise hydrophobic sPS semi-crystalline polymer. The cooperative interaction of sPS with PEG molecules can be conveniently studied by following the formation and evolution of thermoreversible gels of the two polymers from a common hydrocarbon solution.

sPS can form thermoreversible gels in many solvents [26] with the gel junctions consisting either of trans-planar  $\beta$ -form (pastelike opaque gels) or the helical  $\delta$ -form (elastic gels) depending on the solvent used and the heat treatment applied [27]. Besides the sPS case, polymer gels with junctions consisting of crystalline complexes formed by the polymer with the solvent molecules (co-crystals) are specific to polyphenylene oxide (PPO) [28] and, as very recently reported, to poly(L-lactide) (PLLA) [29, 30]. Formation of crystalline pure stereocomplex gels and aerogels of polylactides (PLA) was achieved using the thermoreversible gelation approach followed by solvent exchange, freeze drying and annealing at 70°C as presented in details in [30].

FTIR, XRD and neutron scattering experiments (neutron diffraction and SANS) have shown that the co-crystalline junctions of the elastic gels obtained in chloroform, benzene, toluene or tetrahydrofuran (THF) consist of sPS chains organized to produce a fibrillar morphology as a consequence of trapping the solvent molecules in the cavities between adjacent sPS helices  $(\delta$ -form), which leads to the stabilization of the chains and the suppression of chain folding, thereby promoting the formation of a crystalline phase with a fibrillar morphology [31–33]. From such wet gels, aerogels with tunable porosity can be obtained by special solvent extraction procedures such as freeze drying or the use of supercritical CO<sub>2</sub> to avoid shrinkage and allow the gel network to be preserved [34–36]. Moreover, high-purity nanoporous  $\delta$  and  $\varepsilon$ forms of sPS aerogels can be prepared from their respective gels using a solvent exchange strategy with green solvents followed by an environmentally friendly freeze-drying technique [36]. Due to their highly hydrophobic and oleophilic nature these aerogels could be utilized for the oil-water separation process besides prospected applications in microelectronics, thermal/acoustic insulation, and oil/solvent spill cleanup.

On the other hand, in aerogels produced by supercritical drying of gels made by PEGs with a  $M_{\rm W} > 20~{\rm kg~mol^{-1}}$  and sPS in THF, formation of PEG-rich separate domains, with a size that is a function of the concentration and  $M_{\rm W}$  were evidenced [25]: a low PEG concentration and  $M_{\rm W}$  in the range of 20 kg mol<sup>-1</sup> would yield a superhydrophobic surface of the sPS strands, while at much higher concentration or for  $M_{\rm W} > 100~{\rm kg~mol^{-1}}$  a hydrophilization of PEG-decorated macropores would occur. For a thorough structural characterization of such complex morphologies formed by cooperative gelation of different polymer species upon cooling of their common solution, it is desirable to obtain two or more different pieces of information simultaneously from the same gel sample, which would drastically reduce the ambiguities in interpretation. The

combination of the SANS method, which can provide structural information at the mesoscale and resolve complex hydrocarbon systems based on the powerful contrast variation and matching technique, with FTIR spectroscopy, which can provide information on the conformational state of each polymer species involved in the gelation process, represents a unique approach for such analyses. Recently, we investigated the gels formed in THF by cooperative interaction between sPS and PEG with M<sub>w</sub> between 20 and 40 kg mol<sup>-1</sup> by simultaneous contrasting SANS and FTIR [37]. At lower PEG concentrations in the initial common solution than those discussed in [25], sPS/PEG fibrils were identified and structurally characterized down to 10°C [37]. No PEG crystallization was observed in the IR spectra recorded by in situ FTIR simultaneously with SANS, leading to the conclusion that segments of long PEG molecules are trapped between the co-crystals formed by the sPS chains with solvent molecules ( $\delta$ form) when the temperature is lowered below the sPS gelation point, but the corresponding PEG segments do not adopt a helical conformation typical of pure PEG gels. This unique experimental approach confirmed that PEG molecules with Mw = 20-40 kg mol<sup>-1</sup> assemble together with the co-crystalline gel junctions of sPS and solvent, resulting in PEG decoration of the sPS strands in dried gels. The fact that such high molecular weight PEG molecules do not co-crystallize with the sPS in the crystalline gel junctions is puzzling and motivates further investigation of the structure and conformation of the two polymer species in common gels to gain a clear understanding of their cooperative interaction.

To complete the knowledge of the interaction mechanism and structural behavior of sPS and PEG under common gelation conditions, the case of PEG with very low  $M_{\mathrm{W}}$  was considered in the present work. We report here the characterization of the physical gelation of sPS in the presence of poly(ethylene-glycol-dimethylether) PEGDME ( $M_W = 1.5 \text{ kg mol}^{-1}$ ) from THF solution by simultaneous FTIR and contrast variation SANS, supplemented by ex situ XRD and SEM on drying gels. As in the previous study [37], PEGDME was chosen to avoid clustering effects, which, as reported in [38], depend on the solvent and polymer chain end groups. Based on DSC observations and a detailed SANS analysis, as reported previously [37], the structure and morphology in the single coil conformation of the two polymer species at 50°C and in the ordered regular conformation of sPS in the gel phase at 10°C were characterized by a simultaneous experimental approach of FTIR and SANS. The gel-phase morphology formation as a function of the M<sub>W</sub> of PEGDME, which will be referred to as PEG in the rest of the manuscript, from low  $M_W = 1.5 \text{ kg mol}^{-1}$  to high  $M_W = 40 \text{ kg mol}^{-1}$  and after the subsequent gel-drying process is discussed on the basis of a joint analysis of the SANS, FTIR, XRD, and SEM results.

# 2 | Experimental Section

#### 2.1 | Materials

Syndiotactic polystyrene (sPS) (weight-average molecular weight  $M_{\rm W} \approx 1000~{\rm kg~mol^{-1}}$  and polydispersity around 2.0) was synthesized in both protonated (h-sPS) and deuterated (d-sPS) states according to the coordination polymerization developed by [1], using styrene monomers with a purity of more than 98%, obtained

from Cambridge Isotope Laboratories. PEGDME with  $M_W=1.5$  and 40 kg mol $^{-1}$  were synthesized in both protonated (h-PEGDME) and deuterated (d-PEGDME) states using anionic polymerization and characterized by size exclusion chromatography [39]. These polymers are referred to as PEG1.5 and PEG40 in the following. Tetrahydrofuran (THF) was obtained from Sigma-Aldrich in both protonated (h-THF) and deuterated (d-THF) form and used without further purification.

The polymers were mixed in appropriate amounts in THF to yield solutions with the desired volume fraction (v/v%) of sPS and PEG. The solutions were prepared in sealed flasks, heated to 140°C to allow dissolution of both polymer species, and then cooled to room temperature, where gels formed.

Each gel paste was then transferred to sealed sandwich sample cells with ZnSe windows and a beam path of 1 mm for simultaneous FTIR-SANS analysis. sPS and PEG were also characterized separately in THF solutions, with the gels prepared under the same conditions. To achieve the conditions for matching the neutron contrast between one polymer species and the solvent in the initial solution and to keep the incoherent level at the lowest level, the following combination schemes were used to make only one polymer species "visible" while rendering the other "invisible" in the SANS experiments: i) h-sPS and d-PEG in d-THF, rendering the sPS visible; ii) d-sPS and h-PEG in d-THF, rendering the PEG visible. sPS and PEG alone in d-THF solutions were used in a hydrated state. The neutron scattering length density of these components in hydrogenated and deuterated states is reported in [37].

The polymer solutions prepared for the joint FTIR and SANS characterization contained 5% sPS and 4% PEG1.5 or 1% PEG40. For the XRD and SEM analyses, further gel samples were prepared in THF with the following polymer compositions, using only hydrogenated compounds: 5% sPS; 5% and 4% sPS and PEG1.5, respectively; 5% and 1% sPS and PEG40, respectively; 10% PEG1.5; 10% PEG40.

## 2.2 | Measurements

Simultaneous SANS/FTIR measurements were performed at the China Spallation Neutron Source (CSNS) with the Time-of-Flight (TOF) Multi-slit Very Small Angle Neutron Scattering (MS-VSANS) instrument. SANS and USANS data were collected over a wide Q-range from 0.0003 to 0.5 Å<sup>-1</sup> by combining the standard mode and multi-slit focusing modes of the instrument. A wavelength range from 2.2 to 6.7 Å was used, with three different <sup>3</sup>He tube detectors placed at fixed positions behind the sample, so that neutrons scattered over a wide angular range could be detected simultaneously. The versatile operation of the instrument, including the correction and calibration measurements needed to reduce the experimental data, is described in detail in [40]. A portable JASCO VIR200-FTIR spectrometer with a TGS detector was used simultaneously with SANS studies in an experimental setup at the sample position of the neutron diffractometer, as shown in Figure 1. Precise temperature control of the sample was achieved using Peltier elements, while dry air streams were blown onto the sample during the measurement to prevent water condensation on the ZnSe windows of the sample cuvette. A similar experimental set-up was used in previous experimental investigations of sPS films or gels, as reported in [37].

The reduced and calibrated data collected with different detectors were radially averaged and combined to yield the one-dimensional scattering cross section of the sample in question,  $d\Sigma/d\Omega$  in cm<sup>-1</sup>. The experimental data corrected for the solvent contribution were interpreted in terms of structural models using the SASview analysis software package (https://www.sasview.org/). The modeled curves were convoluted with the corresponding instrumental resolution for each of the measurement modes used, as described in [41].

X-ray diffraction patterns of sPS-PEG, sPS, or PEG gels in THF were measured in the range  $2\theta = 7^{\circ}$  to  $30^{\circ}$  using a Bruker 2nd Gen-D2 Phaser powder diffractometer (Cu source). In this way, gels of sPS, sPS-PEG1.5, sPS-PEG40, PEG1.5, and PEG40 were characterized. To prepare the gels, the corresponding amounts of the polymers were mixed in THF, and the solutions were heated to 140°C in sealed flasks to allow homogeneous dissolution of both polymer types. The solution flasks were brought to 50°C, i.e. above the gelling point of sPS [37] and below the boiling point of THF, and held for a few seconds under a cold water jet to allow the THF vapors to condense. The still liquid solutions were immediately transferred into syringes and stored at room temperature until gels had formed due to the gelling behavior of sPS. The gel slices were collected and analyzed in a series of 2 min XRD measurements carried out during the drying process by evaporation of the solvent in air over a period of 20 min.

Scanning electron microscopy (SEM) characterization of the gel samples was performed using a Thermo-Fischer Quattro S Environmental Scanning Electron Microscope that is operated jointly by the Helmholtz-Zentrum Hereon and the Jülich Center for Neutron Science (JCNS). The sPS, sPS-PEG1.5, and sPS-PEG40 gels prepared for XRD analysis were collected, air-dried for 40 min, sputtered with Pt/Pd 80/20, and stored in a high vacuum at  $1.3 \times 10^{-6}$  mbar overnight prior to SEM examination. The SEM micrographs were taken at a working distance of 10 mm with an emitter current of 16 pA and an acceleration voltage of 10 kV using an Everhart-Thornley detector (ETD) collecting surface near secondary electrons.

## 3 | Results

### 3.1 | FTIR-SANS

**Figure 2** shows examples of IR spectra recorded from the mixed system of h-sPS and dTHF in solution at 50°C (red line) and in gel state at 10°C (blue line). The IR spectra from the mixed system of h-PEG and dTHF (yellow line) and from d-THF (green line) at 50°C are shown in parallel. Due to the sample thickness suitable for SANS measurements, which is too thick for FTIR transmission geometry used in the combined experimental setup of simultaneous FTIR/SANS analysis of polymer solutions and gels, many IR regions are saturated due to the strong bands characteristic of solvents or polymers and only the weak bands are available for investigation (Figure 2a). The spectral ranges at 500–600 cm<sup>-1</sup> and at 1200–1650 cm<sup>-1</sup> can be fully utilized

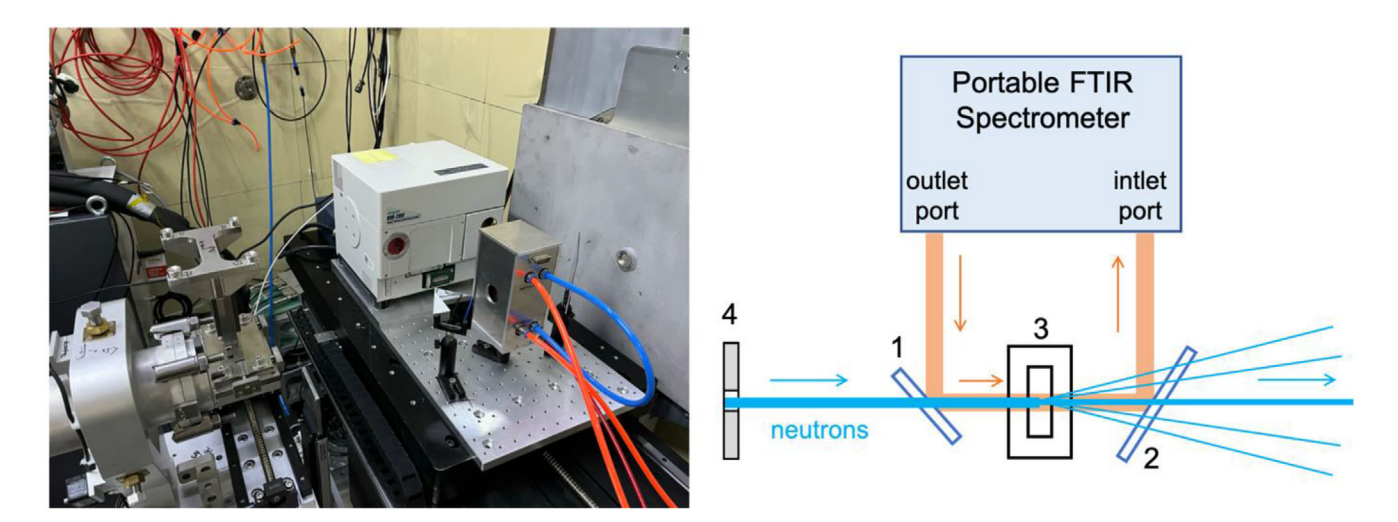


**FIGURE 1** Arrangement of the equipment for simultaneous SANS-FTIR measurements: left—installation of the FTIR spectrometer, the optical system and the sample holder with the temperature control environment at the sample position of the MS-VSANS instrument; right—schematic representation of the arrangement for the FTIR transmission measurement of the sample in the neutron beam: 1, 2 – optical mirrors for reflecting the IR beam and transmitting the neutron beam; 3 – sample container in a temperature-controlled environment; 4 – sample aperture of the neutron scattering instrument; the neutron beam is marked in blue, the IR beam in orange."

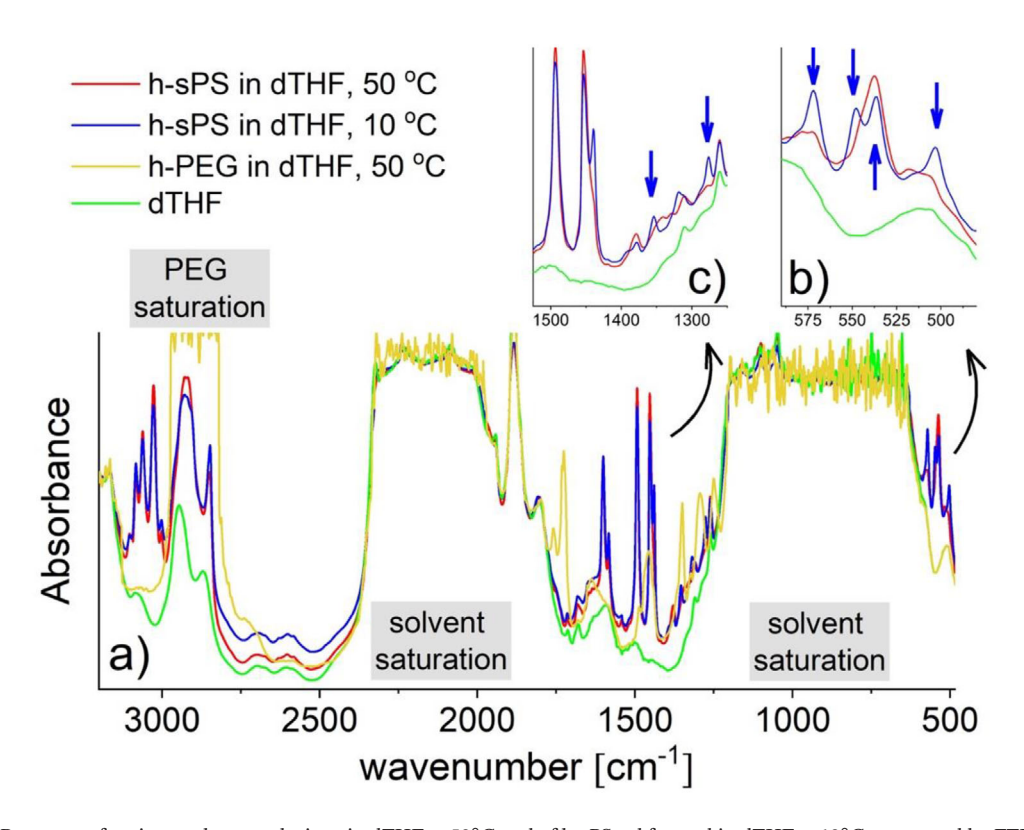


**FIGURE 2** IR spectra of various polymer solutions in dTHF at 50°C and of h-sPS gel formed in dTHF at 10°C, measured by FTIR in transmission geometry with 1 mm thick samples during simultaneous characterization with SANS. Panel (a) shows the complete spectrum with the IR regions saturated due to strong solvent or PEG bands. Panels (b) and (c) show the regions available for IR spectroscopy analysis with examples of the conformational change of sPS chains with the characteristic bands for the helical conformation indicated by the blue arrows.

when mixed solutions of both polymers are investigated upon cooling to 10°C. The first range (Figure 2b) is characteristic of the conformation bands of the h-sPS polymer in the crystalline forms  $\delta$ ,  $\delta_{\rm e}$ , and  $\gamma$  or the non-crystalline glassy or amorphous states, as determined by careful analysis of thin sPS films with a thickness of up to 100  $\mu$ m [5, 11, 42–47]. The frequency range

between 1200 and 1650 cm<sup>-1</sup> (Figure 2c) is another range that is sensitive to conformational changes between different crystalline forms of sPS, as discussed in detail in [11, 47]. The IR bands due to deuterated sPS show frequency shifts compared to hydrated sPS [48]. The vibration modes in which hydrogen atoms are mainly involved show significantly lower frequency shifts, such as the

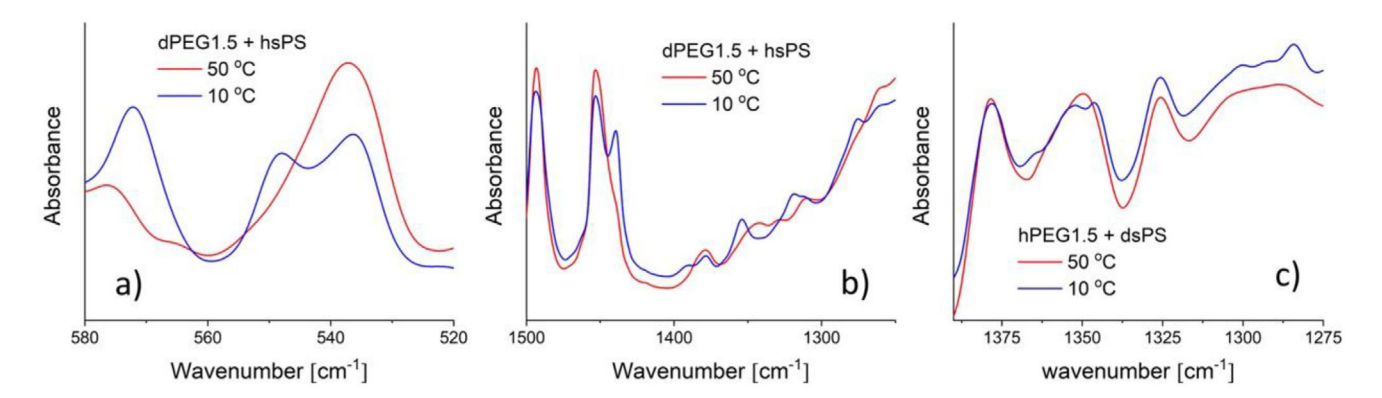


**FIGURE 3** | Selected regions from the FTIR spectra measured at different temperatures simultaneously with SANS on a common sPS and PEG1.5 solution in d-THF, for different neutron contrast conditions, as indicated in the panels.

CH stretching modes, which occur in the range of 3100–2800 cm<sup>-1</sup> in hydrogenated sPS, as shown in Figure 2a, and which shift to the range 2300–2000 cm<sup>-1</sup> in the case of d-sPS, where they cannot be observed due to saturation effects caused by the strong solvent bands. The modes that are mainly due to the shifts of carbon atoms do not show any major shifts. The sPS dissolved at 50°C assumes an amorphous coil conformation characterized by the IR band at 538 cm<sup>-1</sup> (Figure 2a,b), which was associated with the segments of random conformation according to the works discussed in [42, 43].

When the temperature falls below the gelation point, the sPS assumes a helical TTGG conformation, which leads to the fibrillar junctions of the polymer gel, as reported in [31, 37]. This conformation is characterized by the bands at 500, 549, and 572 cm<sup>-1</sup> observed at 10°C in Figure 2b and indicated by the blue arrows. The configuration of the bands is similar to that described in [42–47] for the  $\delta$ -clathrates of sPS, which form when glassy films are exposed to vapors of various solvents. The bands marked by the blue arrows in Figure 2c are characteristic of sPS in the TTGG conformation at 10°C and agree well with the bands discussed in [11, 43] when  $\delta$ -form clathrates of sPS are formed by the exposure of glass films to toluene vapors.

The regions with saturated bands are even broader in the case of h-PEG in dTHF solution (Figure 2a). In addition to the strong solvent bands, the region around the CH<sub>2</sub> stretching band of h-PEG at approximately 2900 cm<sup>-1</sup> [48] also shows saturation, rendering the spectral range unusable for the analysis of samples containing mixed sPS and PEG polymers. In the range 1200–1650 cm<sup>-1</sup> (Figure 2a), the characteristic bands of h-PEG can be observed, which makes this range useful for IR spectroscopic analysis of gel samples containing this polymer [49]. Therefore, FTIR in transmission geometry, performed simultaneously with SANS on thick samples (1 mm beam path), can only be used to investigate limited IR spectral ranges, as shown in Figure 2b,c.

Selected IR bands of the sPS-PEG system in d-THF at two temperatures, 50°C and 10°C, are shown in **Figure 3a**–c, with the two polymers in either the hydrogenated or deuterated state, corresponding to the different contrast conditions used for SANS. Again, the conformational change of the h-sPS from the amorphous single-coil to the helical TTGG in the fibrillar gel junctions is observed in the presence of d-PEG (Figure 3a,b).

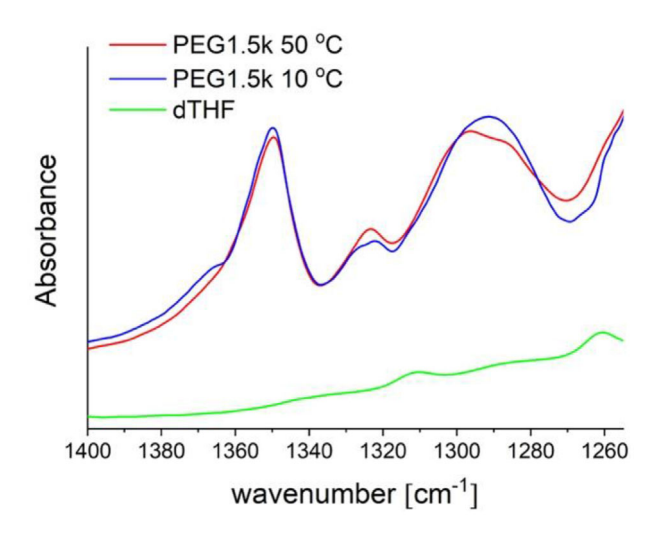


**FIGURE 4** | IR spectra in the conformational band range of PEG1.5 in d-THF, measured at two temperatures, in the solution and incipient gel state.

The characteristic bands of the  $\delta$ -form sPS are the same as those also observed in the sPS alone in dTHF (Figure 2a,b), which proves that the gelation of sPS in cooling to samples down to 10°C accompanied by the conformational change of the polymer is the driving effect of the morphology formation and evolution also in the sPS and PEG common solution in dTHF. On the other hand, the spectra in the PEG conformational bands region (1400 to 1250 cm $^{-1}$ ), where the characteristic bands of h-PEG in amorphous (1352 cm $^{-1}$ ) and helical (1345 and 1364 cm $^{-1}$ ) forms should appear [48, 49], show a weak qualitative change around 1350 cm $^{-1}$  with decreasing temperature from 50°C to 10°C, indicating that PEG1.5 adopts to a little extent a helical conformation when the common sample with the d-sPS is cooled below the sPS gelation temperature.

At 50°C, the IR band characteristic of amorphous PEG is observed at around 1350 cm<sup>-1</sup> (Figure 3c), while at 10°C the splitting that yields the weak band observed at 1345 cm<sup>-1</sup> and the additional weak band at 1364 cm<sup>-1</sup> is indicativ of the helical conformation that the PEG started to adopt. According to [47], the bands at 1327 and 1380 cm<sup>-1</sup> can be assigned to d-sPS. The IR spectra of PEG1.5 alone in dTHF at 50°C and 10°C are shown in **Figure 4**,

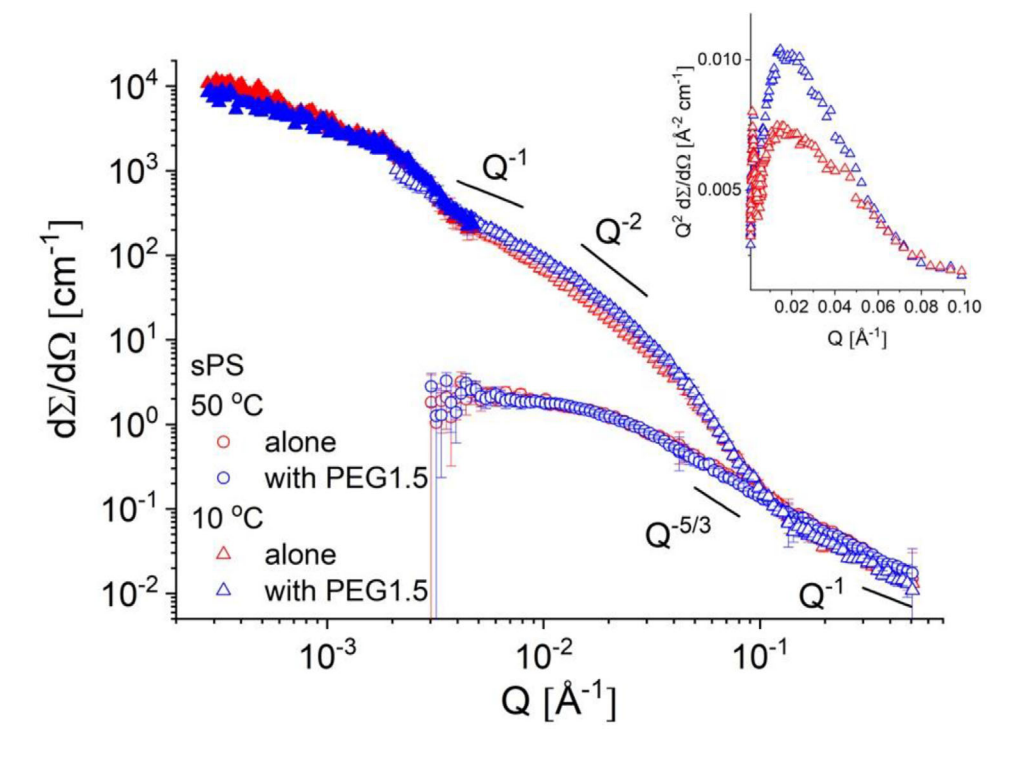


FIGURE 5 | SANS cross sections measured under sPS-visible contrast conditions of sPS and sPS-PEG1.5 systems in dTHF solution at decreasing temperature from the single coil conformation regime at 50°C to the gelation regime of sPS at 10°C shown in log-log representation. The inset shows the data at 10°C in a Kratky plot. The solid black lines show the power law behavior of the scattering intensity in different Q-ranges.

plotted parallel to those of the solvent. Although the spectra are not too different and the band at 1352 cm $^{-1}$  dominates at both temperatures, slight changes in the bands in the range of 1280–1300 cm $^{-1}$  and the appearance of a shoulder at about 1365 cm $^{-1}$  can be observed at  $10^{\circ}$  C, indicating that PEG1. 5 undergoes some conformational changes at low temperature. No strong bands at 1343 and 1242 cm $^{-1}$  attributed to the  $A_2$  modes, and at 1359, 1280, 1150, and 1109 cm $^{-1}$  attributed to the  $E_1$  modes as discussed in [48, 49] are visible in our IR spectra, which indicates that for the polymer  $M_{\rm W}$ , volume fraction and temperature range studied in our current work the PEG chains stay mostly in amorphous conformation in all samples. Based on the weak spectral details observed in Figures 3c and 4. we can assume that only to a little extent PEG crystallization in TTG conformation occurs.

## 3.2 | SANS

SANS patterns of the sPS polymer under neutron contrast conditions, visualizing it either in the mixed solution with PEG1.5 (tuned PEG1.5) or alone in dTHF, are shown in **Figure 5** as collected at 50°C and 10°C over an extended Q-range combining the two measurement modes at the MS-VSANS instrument.

In both sample types, the sPS at 50°C is present in coil form. The Guinier range typical for such a morphology is observed at approximately  $Q=0.02\,\mbox{\normalfont\AA}^{-1}$ . In the absence of any structure factor effects due to correlations between coils in highly concentrated solutions, the radius of gyration  $R_g$  of the polymer coil may be estimated from the model analysis of the transition region between the plateau and the power-law behavior toward high Q. At high Q, the intensity behaves as  $I(Q){\sim}Q^{-p}$ , where the

characteristic decay exponent indicates the quality of the solvent: chains in a theta solvent without interaction with excluded volume form Gaussian coils with a characteristic decay p = 2of the scattering intensity, while chains with excluded volume in a good solvent give an exponent p = 5/3. For semiflexible polymer chains, a transition to Q-1 behavior follows at higher Q, whereby the polymer chain looks like a rod-like segment locally, on the length scale of the persistence length  $l_p$ . The power law behavior of the scattering from the sPS semiflexible single coils at 50°C is indicated in Figure 5 as Q<sup>-5/3</sup> at intermediate Q and Q<sup>-1</sup> at high Q. Fitting such scattering patterns using the unified function of Beaucage [50, 51], as has already been done in the case of PEG20 and PEG40 with high M<sub>W</sub> [37], would yield the "forward scattering" and the  $R_{\scriptscriptstyle g}$  of the ensemble of polymer coils in solution, provided that there is no interaction between the coils. The forward scattering of an ensemble of protonated polymer coils dissolved in deuterated solvent with a volume fraction  $f_P$  is defined as  $I_0 = \phi_P \Delta \rho^2 V_m$ , where  $\Delta \rho$  is the neutron contrast that represents the difference in SLD between the protonated polymer and the deuterated solvent, and V<sub>m</sub> is the molar volume of the polymer chain. However, interpreting the 50°C scattering patterns using the same approach as in [37] yielded a "forward scattering" that is too low compared to that expected from the composition of the sPS solution in dTHF, both in the presence and absence of PEG1. 5. Therefore, structure factor effects that make this analysis inaccurate appear to affect the sPS scattering profiles at 50°C, leading to a suppression of the measured intensity towards lower Q.

At 10°C, the sPC scattering patterns in the two sample types are characterized by a much higher intensity and a more complex profile than at 50°C. As reported in [37], sPS polymer

assemblies apparently form when passing the gelation point polymer towards lower temperatures, resulting in the scattering profiles observed at 10°C. The two 10°C patterns, for sPS alone or in the presence of PEG1.5, look quite similar, although slight changes can be seen at medium Q, where the scattering intensity of SPC in the presence of PEG1.5 is higher than that of sPS alone, as indicated by the Kratky plot of the data in the inset of Figure 5. Furthermore, at very low Q, slight differences can be observed between the sPS scattering patterns in the two sample types (the patterns with solid symbols). For sPS alone in dTHF (red symbols), the intensity level is slightly higher than for sPS in the presence of PEG1.5 (blue symbols). We can only speculate that the morphologies formed by sPC and PEG1.5 are larger than those formed by sPS alone, resulting in scattering features that are "shifted" to lower Q-values.

Qualitatively, one can assume that elongated structures with an overall 1D aspect that exhibit a 2D aspect on a smaller length scale corresponding to their lateral size are formed by the sPS at 10°C, which is similar to the observations reported in [37]. These are fibrillar platelet-like morphologies that give a scattering pattern that behaves as Q<sup>-2</sup> at medium Q and develops into Q<sup>-1</sup> behavior at low Q. The fibrils interconnect to form a largerscale network that provides the scattering at very low Q. At this point, it should be mentioned that the very low Q portion of the scattering patterns shown in Figure 5 were measured at 10°C in a slit geometry (filled symbols as opposed to the empty symbols for the remaining patterns measured in pinhole SANS mode), which smears out the possible scattering characteristics that might otherwise be distinctly seen in the pinhole or focusing lens geometry [52]. Furthermore, due to vertical slit smearing, the overall appearance of the scattering profile becomes a weaker power law of intensity compared to the case of the typical measurement mode using pinhole geometry (i.e., I~Q<sup>-3</sup> instead of  $I \sim Q^{-4}$ ).

Due to this distortion, the slit-smeared data are therefore usually not directly displayed in combination with the pinhole SANS data. However, it is possible to simultaneously fit both VSANS and SANS data sets, taking into account the corresponding instrumental resolution smearing of the model curve. It should also be noted that the scattering patterns measured at 10°C show a similarly high Q behavior as those measured at 50°C, with only a slight decrease in intensity, indicating that most of the sPS still behaves like coils and coexists with the fibrillar morphology. This defines the typical behavior of a gel system, which is a large-scale 3D network consisting of "polymer-poor" regions with loose polymer coils and large pores and "polymer-rich" regions that represent the gel junctions, namely the fibrillar aggregates that crosslink the polymer coils.

**Figure 6** shows the SANS patterns of the PEG1.5 polymer under the neutron contrast conditions that make it visible when mixed with the sPS (when the sPS is match-out) or alone in dTHF. The data were acquired only in the pinhole mode of the MS-VSANS instrument, as the contrast conditions chosen for these measurements provided only a very weak scattering intensity in the focusing mode and did not allow the acquisition of good quality data. Also shown here are scattering patterns collected at 50°C and 10°C (for clarity, the scattering pattern of PEG1.5 alone in dTHF at 50°C, which is similar to that of PEG1.5 in

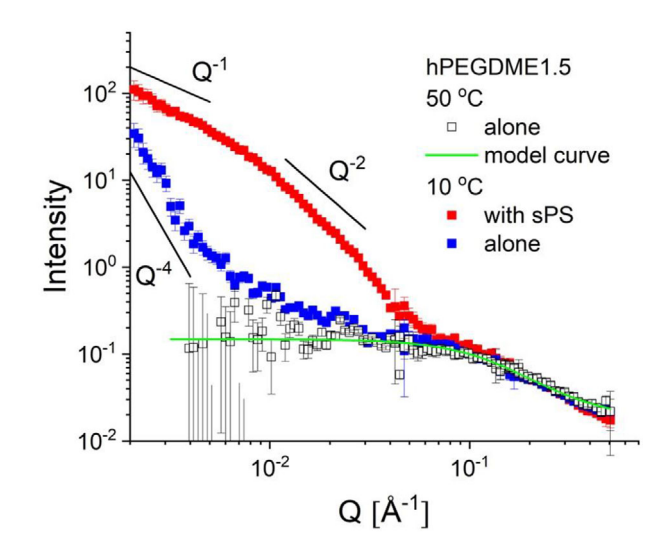


**FIGURE 6** | SANS cross sections measured under PEG1.5-visible contrast conditions of PEG1.5 and sPS-PEG1.5 systems in d-THF solution at decreasing temperature from the single coil conformation regime at 50°C to the gelation regime at 10°C. The solid black lines show the power law behavior of the scattering intensity in different Q-ranges.

the common solution with sPS, has been omitted from Figure 6). Again, the polymer is in a single-coil conformation at  $50^{\circ}$ C, and the scattering patterns show the scattering features characteristic of this morphology. The Guinier regime for short PEG1.5 chains appears at much higher Q compared to the sPS case (Figure 5), indicating a much smaller  $R_g$  for the PEG1.5 in dTHF solution.

As shown in [37], the PEG coils are not affected by correlation effects in the presence of the much higher  $M_{\rm W}$  sPS, so that no structural factor should influence the scattering data. An analysis of the scattering pattern using the unified model of Beaucage [50, 51] gave  $R_{\rm g}=15.62\pm0.02$  Å and the "forward scattering"  $I_0=0.19\pm0.02~{\rm cm}^{-1}$ . The radius of gyration is similar to atomistic MD simulations of PEG molecules of variable length in different solvents [53]. The fitted "forward scattering" is very similar to the scattering calculated for the sample composition, indicating that the PEG1.5 is in coil conformation without coil interactions. The modelled scattering profile is represented by the green curve in Figure 6.

At 10°C, the scattering patterns of PEG1.5 differ significantly from the single coil pattern for different sample compositions, again indicating the formation of larger aggregates containing the PEG1.5 polymer. However, in contrast to sPS (Figure 5), the PEG1.5 scattering patterns are very different depending on the sample type. For PEG1.5 alone in dTHF, a sharp increase in scattering intensity is observed at low Q, which behaves like I(Q)  $\sim Q^{-4}$  (Porod-like scattering), although the scattering profile at medium and high Q is similar to that of the polymer coil. It can be concluded that some PEG1.5 chains are involved in a strong aggregation process at 10°C, probably as a result of weak crystallization effects discussed in the FTIR paragraph, which lead to very large morphologies with sizes outside the Q window used in these measurements. In contrast to the case where PEG1.5 alone is dissolved in dTHF in the initial solution, in the presence of sPS a very strong scattering is obtained, following the general behavior of the scattering pattern visualized by sPS in the same

**TABLE 1** | Parameters delivered by the fitting procedure of the experimental data at 10°C according to the model discussed in the text.

Contrast condition		
Parameter	sPS visible	PEGDME40K visible
I <sub>0</sub> aggregates [cm <sup>-1</sup> ]	$829.43 \pm 25.1$	$91.18 \pm 2.5$
$l_a$ , thickness [Å]	$40.59 \pm 0.95$	$40.59 \pm 0.95$
$l_b$ , width [Å]	$156.53 \pm 4.28$	$140.72 \pm 3.55$
$l_c$ , length [Å]	600, fixed	600, fixed
$I_0 coil [cm^{-1}]$	$3.11 \pm 0.13$	$0.17 \pm 0.008$
R <sub>g</sub> coil [Å]	$67.44 \pm 1.80$	$15.56 \pm 0.98$
$P_3 [cm^{-1} Å^{-3}]$	3.0 E-6	4.0 E-7

sample type: a  $Q^{-2}$  power law behavior is observed at medium Q, evolving to lower O towards  $Q^{-1}$ .

As reported in [31], the gel junctions formed when sPS was mixed with high molecular weight PEG were fibrillar morphologies co-formed by the sPS and PEG chains, with sPS adopting the crystalline helical conformation and PEG adopting an amorphous elongated conformation in the common aggregates. In these samples, both the high molecular weight sPS and PEG exhibited long amorphous segments that emerged from the gel junctions and gave the 3D network aspect of the gel. Under the corresponding neutron contrast conditions visualizing either the sPS or the PEG, the scattering patterns look very similar, the only difference being the intensity, which is much higher in the case of the contrast condition visualizing the sPS (the samples in [37] were prepared for 5% sPS and 1% PEG20 or PEG40, in v/v % in solution). In the current situation of the mixed sPS and PEG1.5 gels, it looks as if the scattering patterns measured in the corresponding contrast condition that visualizes either polymer follow approximately the same behavior, again indicating a common gelation of sPS and PEG1.5 in a common morphology, which is the basic unit (junction) of the gel.

The results of a simultaneous fit of the scattering patterns corresponding to the common sPS-PEG1.5 morphology observed under two contrast conditions by applying the same approach as in the previous study [37], namely using a model combining the form factor of a long parallelepipedon with the coil form factor at high Q values and a  $Q^{-3}$  power law in the very low Q region, are shown in **Figure 7**. The model curves corresponding to the two contrast conditions describe the experimental data quite well. The results of the fitting procedure are shown in **Table 1**.

An attempt was made to adjust the dispersion from the large-scale morphology observed at very low Q values in the VSANS range using a similar approach to that used in the previous study on sPS-PEG40 gels [37]. The USANS data measured with the KWS-2 instrument in lens focusing mode on the sPS-PEG40 gel under contrast conditions, which made the PEG visible, were interpreted using a spherical shape factor that describes the structural feature clearly observed in the scattering data at about  $Q=0.0005~\mbox{Å}^{-1}$  and an additional asymptotic behavior (power law) of the scattering from a much larger morphology with a size outside the Q range covered in the study. The

current data measured in the slit geometry were interpreted using a bimodal distribution of globular (spherical) shape factors with different sizes ( $R_{small}\cong 2000\ \mbox{\normalfont\AA}$  and  $R_{large}\cong 10000\ \mbox{\normalfont\AA}$ ) that were convolved with the instrumental resolution. A background level corresponding to the intensity at the Q transition between the pinhole and slit geometries and originating from the parallelepipeds was taken into account so that the VSANS model data folded with the slit instrument resolution were superimposed on the scattering from the geljunction morphology. The result of the fitting procedure is shown as the yellow curve in Figure 7. When the data are converted to the pinhole geometry, the results are shown by the green curve in Figure 7.

#### 3.3 | SEM

Figure 8 shows the SEM images of the sPS-based dried gels after evaporation of THF in air. The gels formed by sPS alone (Figure 8a) are shown with those formed by sPS in combination with 1% v/v % PEG40 (Figure 8b) or 4% v/v % PEG1.5 (Figure 8c), always with 5% v/v % sPS. sPS fibrils are clearly visible in the dried polymer gel (Figure 8a), whereby the dry gel is generally characterized by polymer strands with a length of about 200-300 nm and a thickness between 20 and 50 nm as well as large pores with a generally well-defined shape. When the long PEG40 is added, the polymer strands in the dried gel become denser and apparently longer and also show a mingling aspect, which consequently leads to smaller pores with irregular shapes. When PEG1.5 is added, the polymer strands show a massive association, forming a kind of "tuft-like morphology" by binding the strands at one end, which leads to a clustering of polymerrich regions and consequently to the appearance of larger pores.

#### 3.4 | XRD

The XRD patterns of the gels formed from sPS with PEG40 and PEG1.5 in THF are shown in **Figure 9**a,b, where the time evolution of the drying process of gel slices in air is followed with a time step of 2 min. The composition of the samples corresponds to that used in the current and previous [37] SANS experiments, namely 5 v/v% sPS with 1 v/v% PEG40 and 4 v/v% PEG1.5. Figure 9c shows the XRD patterns of the PEG40 and PEG1.5 gels formed in THF for a higher polymer volume fraction in the initial solution, 10 v/v%. Samples were collected at  $10^{\circ}\text{C}$  and quickly transferred to the XRD sample tray with an acquisition time of 1 min, which was sufficiently short to prevent the gel from becoming dry.

For the gels of sPS with PEG polymers (Figure 9a,b) as-prepared (wet gel), the diffraction patterns show no Bragg peak, which is due to a small amount of crystallites formed under these compositional conditions. The results of the as-prepared gels are similar to those reported in [54] for sPS gels formed in 1,2-dichloroethane (DCE) at 5 v/v% polymer in the starting solution, in which case the diffraction pattern displayed no Bragg peaks. Brag peaks appear in the diffraction pattern from wet gels first at polymer concentrations higher than 15 v/v% [54].

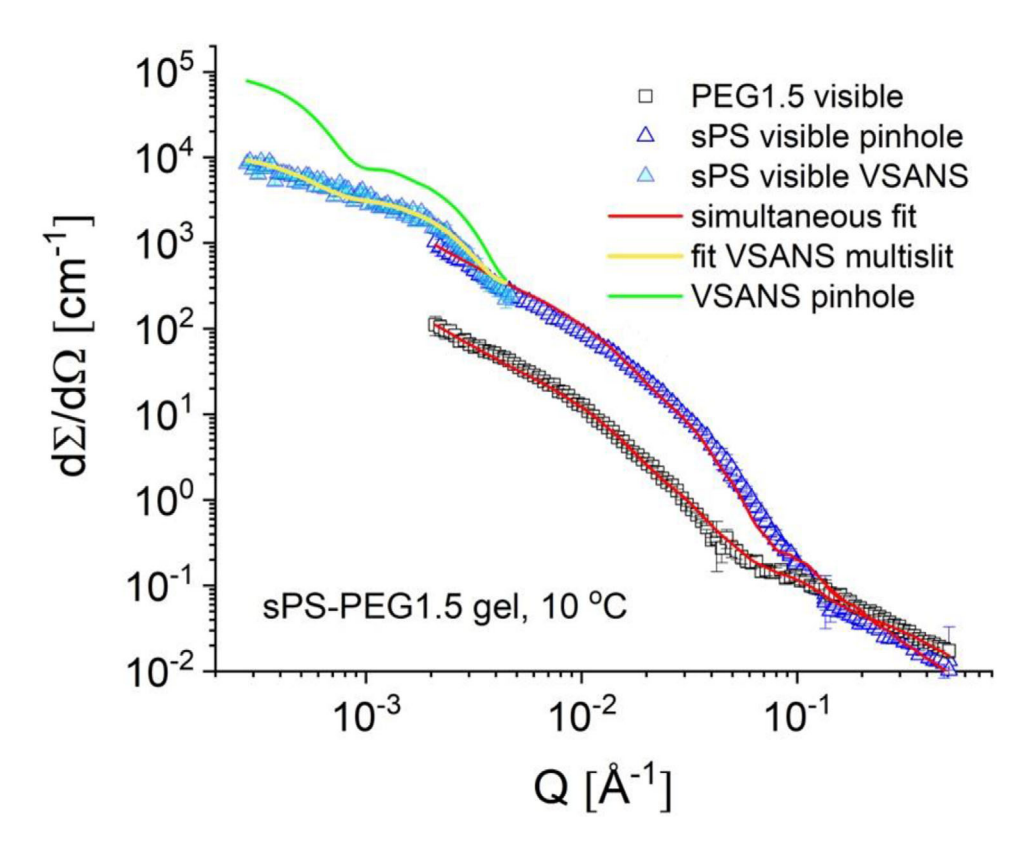


FIGURE 7 | Model interpretation of the SANS patterns of the aggregates formed by gelation of sPS and PEG1.5 in common solution in d-THF at 10°C: the symbols are experimental data measured under different contrast conditions and experimental conditions, as explained in the legend, while the red curves represent the results of simultaneous fitting of both pinhole SANS patterns, as described in the text; the red lines represent the scattering contribution of the aggregates, while the yellow line show the scattering contribution of large-scale morphology convoluted with the slitgeometry instrumental resolution; the green line represent the large-scale morphology scattering contribution convoluted with the pinhole instrumental resolution.

It should be noted that the condition of the prepared gel used for XRD analysis corresponds fairly closely to the condition of the wet gel sample in the SANS experiments. With the evaporation of the solvent, the XRD patterns in Figure 9a,b showed the appearance and development of Bragg peaks as a result of the crystallization of the polymers, up to the final stage observed in the XRD analysis, which corresponds quite closely to the state of the gel sample used in the SEM investigation.

The weak peaks observed at about  $2\theta \approx 8^\circ$  and  $11^\circ$ , together with the stronger peaks developing at about  $2\theta \approx 18^\circ$ ,  $21^\circ$  and  $24^\circ$ , indicated by the arrows in Figure 9a,b, are typical of the crystalline  $\delta$  form of sPS [54], similar to the XRD pattern of clathrate samples of sPS with small organic molecules or of crystalline nanoporous sPS aerogels with isolated ( $\delta$ e) crystalline nanocavities obtained by freeze-drying technique [37]. One should mention here that the fundamental aspects of the polymorphic changes of sPS have been studied on the sPS aerogels as well using variable temperature WAXD [37].

Additional Bragg peaks to those of the  $\delta$  form of sPS can be observed in Figure 9a,b, which can be assigned to the crystalline form of PEG by comparison with the XRD patterns in Figure 9c from the PEG gels. Drying of the gels leads to the morphologies observed in the SEM (Figure 8a–c), which consist of polymer strands with a highly crystalline character.

# 4 | Data Interpretation and Discussion

As previously reported [37], the cooperative gelation of the semicrystalline sPS polymer with PEG polymers in THF and the formation of the common sPS-PEG morphology is determined by the gelation behavior and structural features of sPS. The gel network consists of amorphous, long polymer segments crosslinked by crystalline junctions having a fibrillar morphology and structural features characteristic of the  $\delta$ -crystalline form of sPS. As reported in [24-28] following XRD and ND studies, the fibrillar morphology is a consequence of the co-crystallization of sPS with the solvent molecules in an elongated form, without chain folding. The common morphology formed by sPS and PEG contains crystalline junctions to such a small extent that they do not yield any Bragg peak in the XRD patterns for the small polymer volume fraction considered in this study, which is in good agreement with the observations reported in [54]. This is also in agreement with the SANS results measured at 10°C on the sPS-PEG1.5 gel sample under different contrast conditions, which still contain the typical scattering profile of polymer coils at high Q. This indicates that both the sPS and PEG1.5 polymers in the gel samples are mainly in coil form, with the amorphous long segments emerging from the crystalline junctions. The same explanation applies to the common morphology of sPS and PEG40 studied before [37]. The gel transitions are responsible for the high SANS intensity observed at intermediate and low Q values in Figures 5 and 6. As previously reported in [37],

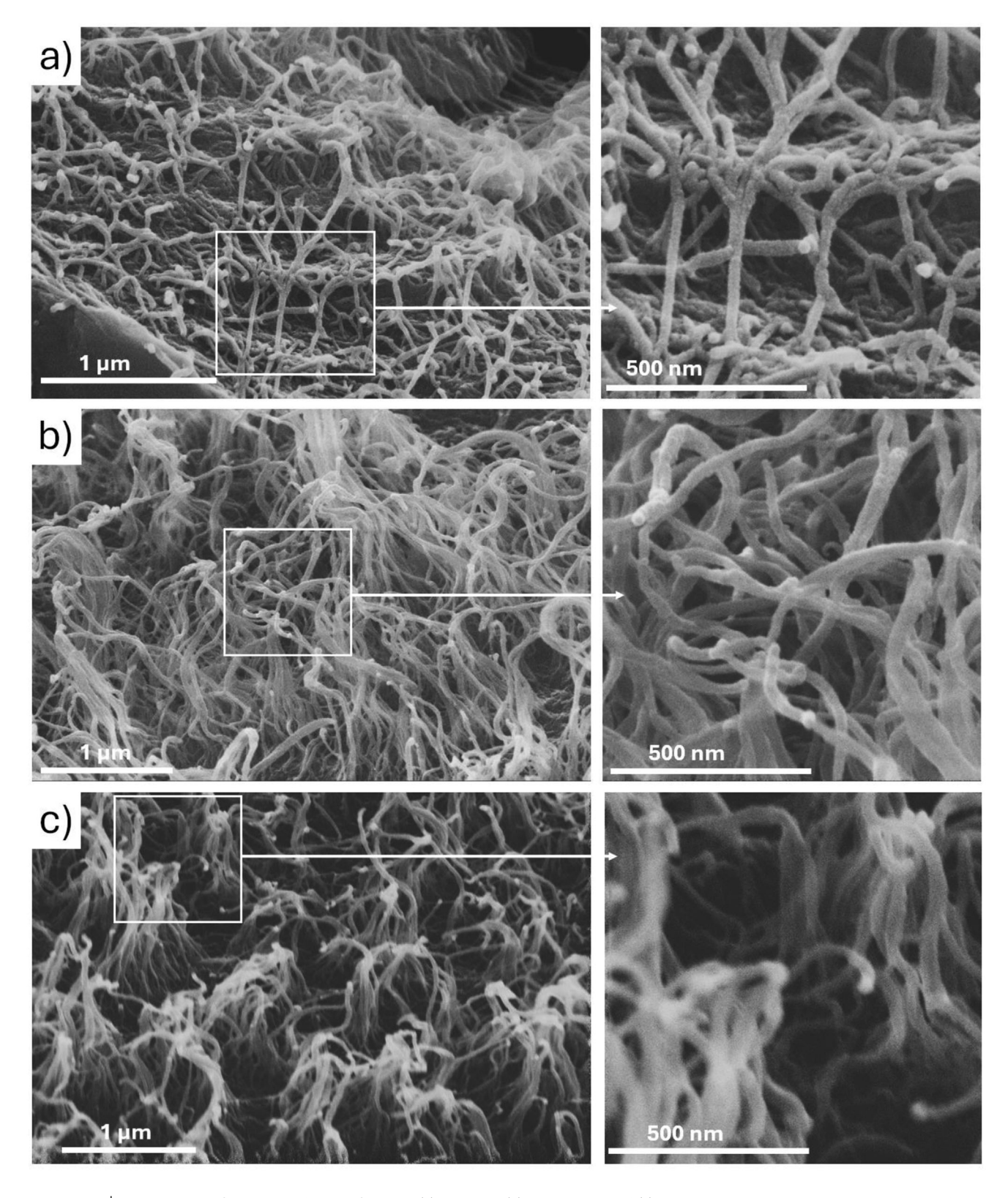
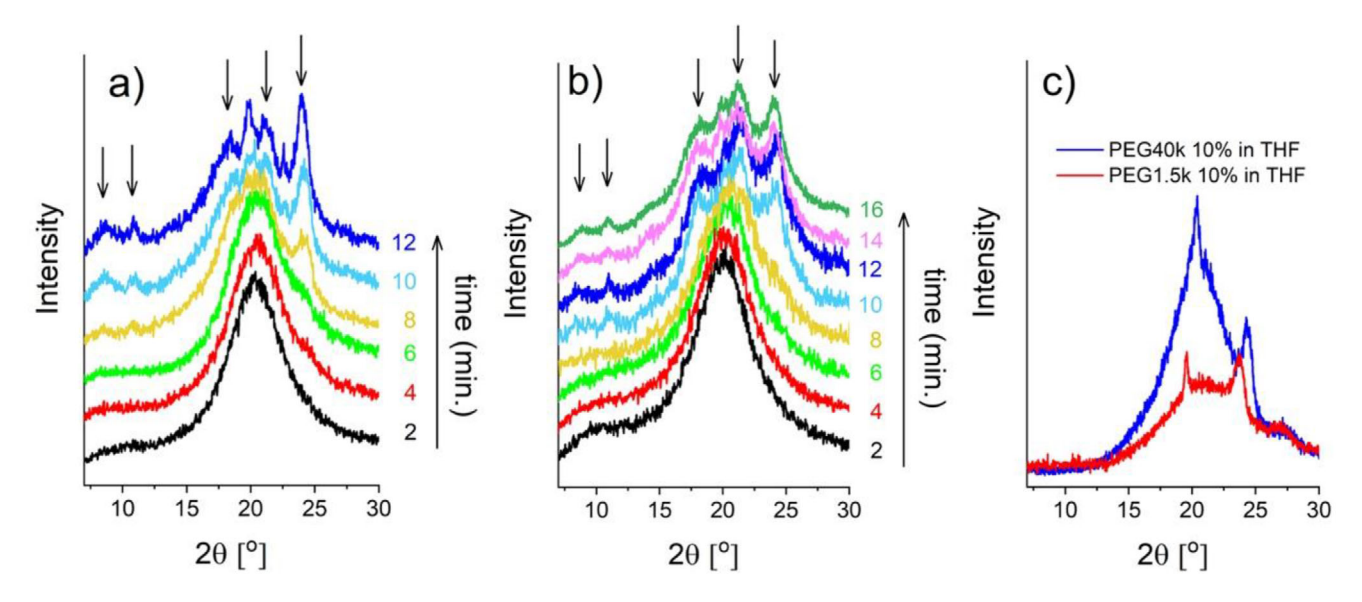


FIGURE 8 | SEM images of dried gels obtained from the (a) gels s-PS, (b) sPS-PEG40, and (c) sPS-PEG1.5. The right-side views show the observed morphology in detail.

the scattering patterns collected from the same sample under different neutron contrast conditions that visualize either the sPS or the PEG components in the common morphology look qualitatively very similar. This is indicative of the co-assembly of sPS and PEG in a common fibrillar morphology and appears

to be the case for both the PEG1.5 considered in this study and the previously investigated PEG40 [37]. The scattering patterns, characterized by a  $Q^{-2}$  power-law behavior at intermediate Q values and evolving towards lower Q values into a  $Q^{-1}$  profile, are typical for fibrillar morphologies.



**FIGURE 9** XRD patterns collected during drying of (a) sPS-PEG40 and (b) sPS-PEG1.5 gels prepared in THF and on PEG gels in THF (c). The time evolution of the drying gels is indicated. Arrows mark the Bragg reflections characteristic of the crystalline  $\delta$ -form of sPS.

Although the basic unit of wet, solvent-containing gels is the same for all three systems discussed here, namely the sPS, sPS-PEG40 and sPS-PEG1.5 in THF, the interaction between the sPS, which is driving the morphology formation and dictating the gel properties, and the PEG molecules appears to be different for these three gel types. This is evidenced by the FTIR and SEM studies of these gels. PEG40 is a long molecule that combines with the sPS to form a common fibrillar morphology in cooling below the sPS gelation point. Although the sPS segments contained in the fibrils change their conformation from an amorphous to a helical conformation as shown by FTIR, the PEG40 does not exhibit this behavior [37]. One can understand this behavior by considering that sPS and solvent molecules co-crystallize by forming fibrils with a  $\delta$ form structure without the sPS chain folding, while formation of this morphology is entrapping segments of the long PEG that may adopt an extended but not a helical conformation. Long amorphous PEG segments of these entrapped chain segments still surround the crystalline junction, which together with the amorphous sPS segment provide a screening for further conformational changes and also the impossibility of the PEG to diffuse out of the junctions. As a result, these segments of both sPS and PEG40 surrounding the crystalline junctions collapse and form the dense and long crystalline strands (according to XRD) that intermingle in the dried gels (Figure 8b), in contrast to the pure sPS gel, which forms shorter and well-defined polymer strands and larger pores (Figure 8a). A completely different behavior seems to be responsible for the interactions in the sPS-PEG1.5 gel. PEG1.5 is a short molecule with a length of about 100 Å when it is in a helical, elongated conformation. Like PEG40, PEG1.5 co-assembles with the sPS fibrils ( $\delta$ -form clathrates with THF molecules, without sPS chain folding) in a common morphology. However, according to FTIR, PEG1.5 changes its conformation from an amorphous to a helical one to some extent. We can assume that the short PEG molecules may undergo a co-crystallization with the sPS by replacing to some extent the solvent molecules entrapped between the sPS helices. Another explanation is that some PEG1.5 molecules undergo a limited crystallization at 10°C subsequent to formation of the

main common sPS and PEG1.5 fibrillar morphology in decreasing temperature below the sPS gelation point.

It should be mentioned here that earlier SANS investigations have shown that the short PEG molecules with  $M_W = 0.5$  and 1 kg mol<sup>-1</sup> can be taken up by the sPS crystal lamellae between the sPS helices when they are incorporated into the uniaxially deformed sPS thin films via the guest exchange process with earlier guest molecules, either chloroform or acetone [24]. The short PEG chains incorporated by the sPS lamellae form an oriented arrangement that is predetermined by the oriented sPS crystal planes in the uniaxially deformed films, which was confirmed by the observation of an anisotropic scattering pattern in contrast variation SANS experiments [24]. In that case, the IR spectra showed no clear helical conformation of the short PEG molecules, even though the PEG was located between the sPS helices. This was attributed to a high diffusing behavior that allowed the short PEGs to penetrate trough the sPS lamellae during the guest exchange process and occupy the cavities between the sPS helices. However, after exposure of the films to increasing temperatures up to 100°C, the short PEGs also diffuse out of the sPS lamellae, as demonstrated by the XRD results, which indicate the presence of the empty  $\gamma$ -form of sPS after thermal treatment of the sPS films [24]. These processes indicate greater mobility of the short PEG chains, which do not adopt a helical conformation even in the sPS lamellae. However, the current case of PEG1.5 appears to differ from the case of PEG0.5 and PEG1 described in [24]. Apparently, after the formation of the gel compounds, PEG1.5 undergoes limited and localized crystallization, which connects the already formed common sPS and PEG morphologies during gelation of sPS. This localized crystallization of PEG1.5 could explain the bonding of the polymer crystal strands in the dry gel in a "tuft-like morphology," as seen in the SEM image in Figure 8c.

The incorporation of PEG molecules into sPS gels leads to polymer nanocomposites that can make sPS hydrophilic. sPS aerogels, which are inherently hydrophobic, could have potential for moisture absorption and particle removal if a certain degree

of hydrophilicity is achieved through appropriate preparation, in which the concentration and molecular weight of the PEG and the gel production process are varied. As discussed in [25], the use of PEG with very high  $M_{\rm W}$  (>100 kg mol $^{-1}$ ) can lead to hydrophilic pores in sPS aerogels. The current study shows that PEG with low and very low  $M_{\rm W}$  also yields interesting morphologies in the sPS gels, whose potential should be further investigated, using higher PEG concentrations than those used in this work to fully understand the interaction mechanism between the two polymer types.

#### 5 | Conclusions

The gelation of sPS in the presence of low molecular weight PEGDME ( $M_W = 1.5 \text{ kg mol}^{-1}$ ) from THF solution was investigated by simultaneous contrast variation (SANS) and FTIR spectroscopy on wet gels, complemented by XRD and SEM on dried gels. Contrast matching SANS was used to follow the behavior of each polymer species during the transition from the coil conformation of both polymers in the solution state to the ordered regular conformation of sPS in the gel state. A common morphology of sPS and low Mw PEGDME if generated as a consequence of the gelation tendency of sPS at high temperatures around 40°C, with the crystalline junctions of the gel occurring due to co-crystallization behavior of sPS with the solvent molecules. The sPS changes from the amorphous coil to the helical TTGG conformation when the gelation temperature is crossed, forming a fibrillar morphology with a local 2D aspect. This morphology represents the junctions of the large length-scale network morphology of the gel. It was found that unlike the high molecular weight PEGDME chains, which are entrapped by the sPS fibrils without changing their amorphous conformation, the shorter PEGDME with a Mw of 1.5 kg mol<sup>-1</sup> co-crystallizes with the sPS in the common gel junctions to a certain extent showing a limited conformational change to a helical form. Drying of the gels by evaporation of the solvent in air was monitored by XRD, and time-resolved formation and evolution of the crystalline domains revealed that both the sPS and PEG crystallize over time, yielding the polymer strands observed by SEM. Although the basic unit of the gel, the crystalline junction, is quite similar for the sPS gel and the common sPS-PEGDME gels regardless of the M<sub>W</sub> of PEGDME, the morphology of the larger scale dry gels differs greatly between these three types of systems. It appears that the mechanism of cooperative gelation between the PEGDME and sPS molecules depends on the molecular length of the PEGDME, which also determines the macroaggregated aspect of the dried gel. While the sPS drying gel shows a rather homogeneous distribution of polymer strands and well-defined pores, the dry gel containing the high M<sub>w</sub> PEGDME is characterized by denser strands and smaller, irregularly shaped pores. The long amorphous PEGDME segments, which emerged out of the crystalline junctions together with amorphous sPS segments, collapsed and crystallized as the gel dried, resulting in a more irregular appearance of the desiccated gel than in the case of sPS alone. In gels containing low M<sub>w</sub> PEGDME, several polymer strands join together at one end to form "tuft-like" macro-arrangements due to the additional cocrystallization of PEGDME with sPS, which results in very large pores.

Knowledge of all the structural features that characterize the gel morphology on small and large length scales helps to understand the interaction of the sPS with PEGs of different molecular weights as well as the location and conformation of the PEG molecules, which can ultimately be used to optimize the way of making the sPS hydrophilic to a certain degree.

#### Acknowledgements

A.R. thanks John Barker (NIST) for the useful discussions on how to handle the instrumental resolution of the slit geometry SANS when fitting the experimental data. A.R. thanks the staff members of the Very Small Angle Neutron Scattering at the China Spallation Neutron Source (CSNS) (https://cstr.cn/31113.02.CSNS.VSANS), for providing technical support and assistance in data collection and analysis.

#### **Conflicts of Interest**

The authors declare no conflict of interest.

#### **Data Availability Statement**

The data that support the findings of this study are available from the corresponding author upon reasonable request.

#### **References:**

- 1. N. Ishihara, T. Seimiya, M. Kuramoto, and M Uoi, "Crystalline Syndiotactic Polystyrene," *Macromolecules* 19 (1986): 2464–2465.
- 2. G. Guerra, V. M. Vitagliano, C. De Rosa, V. Petraccone, and P. Corradini, "Polymorphism in Melt Crystallized Synditoactic Polystyrene Samples," *Macromolecules* 23 (1990): 1539–1544.
- 3. Y. Chatani, Y. Shimane, Y. Inoue, T. Inagaki, T. Ishioka, T. Ijitsu, and T. Yukinari, "Structural Study of Syndyotactic Polystyrene: 1. Polymorphism," *Polymer* 33 (1992): 488–492.
- 4. E. Bhoje Gowd, K. Tashiro, and C. Ramesh, "Structural Phase Transitions of Syndiotactic Polystyrene," *Progress in Polymer Science* 34 (2009): 280–315.
- 5. E. Bhoje Gowd, N. Shibayama, and K. Tashiro, "Structural Changes in Thermally Induced Phase Transition of Uniaxially Oriented  $\delta$ e Form of Syndiotactic Polystyrene Investigated by Temperature-Dependent Measurements of X-Ray Fiber Diagrams and Polarized Infrared Spectra," *Macromolecules* 39 (2006): 8412–8418.
- 6. O. Tarallo, M. M. Schiavone, V. Petraccone, C. Daniel, P. Rizzo, and G. Guerra, "Channel Clathrate of Syndiotactic Polystyrene With p-nitroaniline," *Macromolecules* 43 (2010): 1455–1466.
- 7. O. Tarallo, M. M. Schiavone, and V. Petraccone, "Polymorphism of the co-crystalline Forms of Syndiotactic Polystyrene with Chloroform: Crystal Structure of the  $\delta$  Clathrate," *European Polymer Journal* 46 (2010): 456–464.
- 8. O. Tarallo, M. M. Schiavone, and V. Petraccone, "Structural Characterization of the d-clathrate Forms of Syndiotactic Polystyrene with n-alkanes," Polymer~52~(2011):~1426-1435.
- 9. A. Yoshioka and K. Tashiro, "Infrared Bands Sensitive to the Chain Packing Mode in the Crystalline  $\delta$ ,  $\delta$ e, and  $\gamma$  Forms of Syndiotactic Polystyrene," *Macromolecules* 36 (2003): 3001–3003.
- 10. P. Shaiju and E. Bhoje Gowd, "Factors Controlling the Structure of Syndiotactic Polystyrene Upon the Guest Exchange and Guest Extraction Processes," *Polymer* 56 (2015): 581–589.
- 11. Bhoje Gowd, S. S. Nair, C. Ramesh, and K. Tashiro, "Studies of the Clathrate ( $\delta$ ) Form of Syndiotactic Polystyrene Crystallized by different Solvents Using Fourier Transform Infrared Spectroscopy," *Macromolecules* 36 (2003): 7388–7397.

- 12. Y. Uda, F. Kaneko, and T. Kawaguchi, "Guest Exchange Process in Syndiotactic Polystyrene Thin Films Measured by ATR-FTIR Spectroscopy," *Polymer* 45 (2004): 2221–2229.
- 13. Y. Uda, F. Kaneko, and T. Kawaguchi, "Guest Exchange Mechanism in the Clathrate Phase of Syndiotactic Polystyrene," *Macromolecules* 38 (2005): 3380–3385.
- 14. F. Kaneko, A. Radulescu, and K. Ute, "Time-resolved SANS studies on guest exchange processes in co-crystals of syndiotactic polystyrene," *Polymer* 54 (2013): 3145–3149.
- 15. K. Kaneko, A. Radulescu, and K. Ute, "Time-resolved Small-angle Neutron Scattering Study on Guest-exchange Processes in co-crystals of Syndiotactic Polystyrene," *Journal of Applied Crystallography* 47 (2014): 6–13
- 16. R. C. Jose, P. Shaiju, B. Nagendra, and E. Bhoje Gowd, "Influence of Host Preparation Method on the Structural Phase Transitions of Syndiotactic Polystyrene Upon the Guest Exchange With n-alkanes," *Polymer* 54 (2013): 6617–6627.
- 17. C. Daniel, A. R. Albunia, C. D'Aniello, P. Rizzo, V. Venditto, and G. Guerra, "Polymer co-crystalline Films for Photonics," *Journal of European Optical Society—Rapid Publication* 4 (2009): 09037
- 18. P. Stegmaier, A. De Girolamo Del Mauro, V. Venditto, and G. Guerra, "Optical Recording Materials Based on Photoisomerization of Guest Molecules of a Polymeric Crystalline Host Phase," *Advanced Materials* 17 (2005): 1166–1168.
- 19. M. Giordano, M. Russo, A. Cusano, G. Mensitieri, and G. Guerra, "Syndiotactic Polystyrene Thin Film as Sensitive Layer for an Optoelectronic Chemical Sensing Device," *Sensors and Actuators B: Chemical* 109 (2005): 177–184.
- 20. P. Rizzo, C. Daniel, and G. Guerra, "Chiro-optical Materials Based on a Racemic Polymer," *Macromolecules* 43 (2010): 1882–1887.
- 21. G. Milano and G. Guerra, "Understanding at Molecular Level of Nanoporous and co-crystalline Materials Based on Syndiotactic Polystyrene," *Progress in Materials Science* 54 (2009): 68–88.
- 22. F. Kaneko and K. Sasaki, "Crystalline Complex of Syndiotactic Polystyrene With Poly(ethylene Glycol) Dimethyl Ethers," *Macromolecular Rapid Communications* 32 (2011): 988–993.
- 23. F. Kaneko, N. Seto, S. Sato, A. Radulescu, M. M. Schiavone, J. Allgaier, and K. Ute, "Development of a Simultaneous SANS/FTIR Measuring System," *Chemistry Letters* 44 (2015): 497-499.
- 24. F. Kaneko, N. Seto, S. Sato, A. Radulescu, M. M. Schiavone, J. Allgaier, and K. Ute, "Simultaneous Small-angle Neutron Scattering and Fourier Transform Infrared Spectroscopic Measurements on Cocrystals of Syndiotactic Polystyrene With Polyethylene Glycol Dimethyl Ethers," *Journal of Applied Crystallography* 49 (2016): 1420.
- 25. X. Wang and S. C. Jana, "Tailoring of Morphology and Surface Properties of Syndiotactic Polystyrene Aerogels," *Langmuir* 29 (2013): 5589–5598.
- 26. C. Daniel, A. Menelle, A. Brulet, and J-M. Guenet, "Thermoreversible Gelation of Syndiotactic Polystyrene in Toluene and Chloroform," *Polymer* 38 (1997): 4193–4199.
- 27. C. Daniel, A. Avallone, and G. Guerra, "Syndiotactic Polystyrene Physical Gels: Guest Influence on Structural Order in Molecular Complex Domains and Gel Transparency," *Macromolecules* 39 (2006): 7578–7582.
- 28. C. Daniel, S. Longo, G. Fasano, J. G. Vitillo, and G. Guerra, "Nanoporous Crystalline Phases of Poly(2,6-Dimethyl-1,4-phenylene) Oxide," *Chemistry of Materials* 23 (2011): 3195–3200.
- 29. N. M. Praveena, G. Virat, V. G. Krishnan, and E. Bhoje Gowd, "Stereocomplex Formation and Hierarchical Structural Changes During Heating of Supramolecular Gels Obtained By Polylactide Racemic Blends," *Polymer* 241 (2022): 124530.
- 30. V. G. Krishnan, N. M. Praveena, R. B. Amal Raj, K. Mohan, and E. B. Gowd, "Thermoreversible Gels of Poly(L-lactide)/Poly(D-Lactide) Blends:

- A Facile Route to Prepare Blend  $\alpha$ -Form and Stereocomplex Aerogles," *ACS Applied Polymer Materials* 5 (2023): 1556–1564.
- 31. C. Daniel, M. D. Deluca, J-M. Guenet, A. Brulet, and A. Menelle, "Thermoreversible Gelation of Syndiotactic Polystyrene in Benzene," *Polymer* 37 (1996): 1273–1280.
- 32. J-M. Guenet, "Microfibrillar Networks: Microfibrillar Networks: Polymer Thermoreversible Gels vs Organogels," *Macromolecular Symposia* 241 (2006): 45–50.
- 33. S. Malik, C. Rochas, M. Schmutz, and J-M. Guenet, "Syndiotactic Polystyrene Intercalates from Naphtalene Derivatives," *Macromolecules* 38 (2005): 6024–6030.
- 34. C. Daniel, S. Giudice, and G. Guerra, "Syndiotacitc Polystyrene Aerogels with B, g and e Crystalline Phases," *Chemistry of Materials* 21 (2009): 1028–1034.
- 35. C. Daniel, S. Longo, R. Ricciardi, E. Reverchon, and G. Guerra, "Monolithic Nanoporous Crystalline Aerogels," *Macromolecular Rapid Communications* 34 (2013): 1194–1207.
- 36. V. G. Krishnan, A. M. Joseph, S. K. Peethambharan, and E. Bhoje Gowd, "Nanoporous Crystalline Aerogels of Syndiotactic Polystyrene: Polymorphism, Dielectric, Thermal, and Acoustic Properties," *Macromolecules* 54 (2021): 10605–10615.
- 37. F. Kaneko, M. M. Schiavone, H. Iwase, S. Takata, J. Allgaier, and A. Radulescu, "Microstructural Investigation of the Cooperative Gelation of Syndiotactic Polystyrene and High  $M_{\rm W}$  Polyethylene Glycol Di-methyl Ether in Common Solution in THF," *Polymer* 295 (2024): 126771.
- 38. B. Hammouda, D. L. Ho, and S. Kline, "Insight Into Clustering in Poly(ethylene oxide) Solutions," *Macromolecules* 37 (2004): 6932–6937.
- 39. C. H. Hövelmann, S. Gooßen, and J. Allgaier, "Scale-Up Procedure for the Efficient Synthesis of Highly Pure Cyclic Poly(ethylene glycol)," *Macromolecules* 50 (2017): 4169–4179.
- 40. T. Zuo, Z. Han, C. Ma, S. Xiao, X. Lin, Y. Li, F. Wang, Y. He, Z. He, J. Zhang, G. Wang, and H. Cheng, "The Multi-slit Very Small Angle Neutron Scattering Instrument at the China Spallation Neutron Source," *Journal of Applied Crystallography* 57 (2024): 380.
- 41. Z. Han, C. Ma, H. Zhu, T. Cui, T. Zuo, and H. Cheng, "The Smearing Function for a Multi-slit Very Small Angle Neutron Scattering Instrument," *Journal of Applied Crystallography* 57 (2024): 1772.
- 42. M. Kobayashi, T. Nakaoki, and N. Ishihara, "Molecular Conformation in Glasses and Gels of Syndiotactic and Isotactic Polystyrenes," *Macromolecules* 23 (1990): 78–83.
- 43. M. Kobayashi, T. Yoshioka, M. Imai, and Y. Itoh, "Structural Ordering on Physical Gelation of Syndiotactic Polystyrene Dispersed in Chloroform Studied by Time-Resolved Measurements of Small Angle Neutron Scattering (SANS) and Infrared Spectroscopy," *Macromolecules* 28 (1995): 7376–7385.
- 44. P. Musto, G. Mensiteri, S. Cotugno, G. Guerra, and V. Venditto, "Probing by Time-Resolved FTIR Spectroscopy Mass Transport, Molecular Interactions, and Conformational Ordering in the System Chloroform—Syndiotactic Polystyrene," *Macromolecules* 35 (2002): 2296–2304.
- 45. K. Tashiro, Y. Ueno, A. Yoshioka, and M. Kobayashi, "Molecular Mechanism of Solvent-Induced Crystallization of Syndiotactic Polystyrene Glass. 1. Time-Resolved Measurements of Infrared/Raman Spectra and X-ray Diffraction," *Macromolecules*, 34 (2001): 310–315.
- 46. T. Nakaoki and M. Kobayashi, "Local Conformation of Glassy Polystyrenes With Different Stereoregularity," *Journal of Molecular Structure* 655 (2003): 343–349.
- 47. S. Moyses and S. J. Spells, "Conformationally Sensitive Infrared Vibrations of the Syndiotactic Polystyrene/Ethylbenzene Complex," *Macromolecules* 32 (1999): 2684–2689.

- 48. H. Tadokoro, Y. Chatani, T. Yoshihara, S. Tahara, and S. Murahashi, "Structural studies on polyethers, [-(CH2)m-O-]n. II. Molecular Structure of Polyethylene Oxide," *Die Makromolekulare Chemie* 73 (1964): 109–127.
- 49. M. Kobayashi and K. Kitagawa, "Microstructure of Poly(ethylene oxide) Gels Dispersed in Various Organic Solvents," *Macromolecular Symposia* 114 (1997): 291–296.
- 50. G. Beaucage, "Approximations Leading to a Unified Exponential/Power-Law Approach to Small-Angle Scattering," *Journal of Applied Crystallography* 28 (1995): 717.
- 51. B. Hammouda, "Analysis of the Beaucage Model," *Journal of Applied Crystallography* 43 (2010): 1474.
- 52. A. Radulescu, "Intensity Enhancement and Q-Range Extension in Pinhole SANS Instruments with Neutron Focusing Lenses," *Quantum Beam Sci* 9 (2025): 6.
- 53. C. W. Nyambura, J. Sampath, E. Nance, and J. Pfaendtner, "Exploring Structure and Dynamics of the Polylactic-co-glycolic Acid-polyethylene Glycol Copolymer and its Homopolymer Constituents in Various Solvents Using All-Atom Molecular Dynamics," *Journal of Applied Polymer Science* 139 (2022): 52732.
- 54. C. Daniel, G. Guerra, and P. Musto, "Clathrate Phase in Syndiotactic Polystyrene Gels," *Macromolecules* 35 (2002): 2243–2251.